Pairing tendencies in a two-orbital Hubbard model in one dimension

N. D. Patel, A. Nocera, G. Alvarez, A. Moreo, and E. Dagotto

Phys. Rev. B **96**, 024520 — Published 31 July 2017

DOI: 10.1103/PhysRevB.96.024520

Pairing Tendencies in a Two-orbital Hubbard Model in One Dimension

N. D. Patel,[1,2] A. Nocera,[1,2] G. Alvarez,[3] A. Moreo,[1,2] and E. Dagotto[1,2]

[1]*Department of Physics and Astronomy, The University of Tennessee, Knoxville, Tennessee 37996, USA*
[2]*Materials Science and Technology Division, Oak Ridge National Laboratory, Oak Ridge, Tennessee 37831, USA*
[3]*Computer Science & Mathematics Division and Center for Nanophase Materials Sciences, Oak Ridge National Laboratory, Oak Ridge, Tennessee 37831, USA*

The recent discovery of superconductivity under high pressure in the ladder compound $BaFe_2S_3$ has opened a new field of research in iron-based superconductors with focus on quasi one-dimensional geometries. In this publication, using the Density Matrix Renormalization Group technique, we study a two-orbital Hubbard model defined in one dimensional chains. Our main result is the presence of hole binding tendencies at intermediate Hubbard U repulsion and robust Hund coupling $J_H/U = 0.25$. Binding does not occur neither in weak coupling nor at very strong coupling. The pair-pair correlations that are dominant near half-filling, or of similar strength as the charge and spin correlation channels, involve hole-pair operators that are spin singlets, use nearest-neighbor sites, and employ different orbitals for each hole. The Hund coupling strength, presence of robust magnetic moments, and antiferromagnetic correlations among them are important for the binding tendencies found here.

I. INTRODUCTION

High critical temperature superconductors based on iron represent one of the most important open problems in condensed matter physics [1–7]. Early considerations based on Fermi surface nesting provided a robust starting point to rationalize their properties. However, the effect of repulsion between electrons cannot be neglected [6] as exemplified by the existence of large magnetic moments at room temperature [8, 9], superconducting materials without hole pockets [10], as well as unexpectedly complex spin arrangements [7]. Electronic correlation effects must be incorporated to understand the plethora of challenging results that experiments are rapidly unveiling.

A new avenue of research for progress in the iron superconductors family has recently opened. It has been shown experimentally that $BaFe_2S_3$ [11–13], becomes superconducting at pressures above 10 GPa with an optimal critical temperature $T_c = 24$ K. What is remarkable is that this material is not layered, like all other iron-based superconductors, but instead has the geometry of a two-leg ladder. In other words, they have a dominant crystal structure involving pairs of chains, "legs", that are coupled via bonds of strength similar to those along the legs, dubbed the "rungs". This same compound, but at ambient pressure, is a Mott insulator with magnetic order involving ferromagnetic (FM) rungs and antiferromagnetic (AFM) legs and a Néel temperature ~ 120 K [11]. Being the first iron-based superconductor that does not rely on layers, this discovery is conceptually exciting. From the theory perspective one-dimensional systems are often simpler than layers due to the availability of powerful computational techniques, thus robust many-body progress can be achieved in one dimension.

It is important to remark that there are other iron-based ladder materials with intriguing magnetic properties, although they have not been reported to be superconducting at high pressures yet. For example, the two-leg ladder $BaFe_2Se_3$ [14–23] is an insulator, with an activation energy 0.13-0.178 eV [15, 17], long-range AFM order at $\sim$250 K, and robust low-temperature magnetic moments $\sim 2.8\ \mu_B$ [14–16]. The dominant magnetic order at low temperature involves 2×2 iron blocks with their moments aligned, coupled antiferromagnetically along the legs [14, 17]. For the case of KFe_2Se_3, another two-leg ladder material, the magnetic state is as in $BaFe_2S_3$ with FM rungs and AFM legs [18]. These same magnetic states were also found theoretically using the Hartree Fock approximation [20]. Their origin is non-trivial: the 2×2 FM iron block patterns arise from frustration effects between fully FM tendencies at very large Hund coupling and AFM tendencies in all directions at small Hund coupling [20]. Hartree-Fock results for layers [24] and chains [25] also revealed a similarly complex landscape of possible competing magnetic states once interactions are incorporated.

For proper context, it is necessary to recall that in the context of the copper-oxide high-T_c superconductors, the theoretical and experimental study of two-leg ladder compounds made a considerable impact. In general, theorists can produce accurate results for quasi-one-dimensional systems and the early predictions of subtle quantum effects, such as spin gaps and superconducting tendencies upon doping [26–28], were later confirmed experimentally. For instance, high pressure experiments for the two-leg ladder compound $Sr_{0.4}Ca_{13.6}Cu_{24}O_{41.84}$, reported a superconducting critical temperature of 12 K [29]. A quantitative difference between Cu- and Fe-based ladders is that the bridge between coppers is via an oxygen along the Cu-Cu bond, while in chalcogenides the bridge between irons is via chalcogen atoms located up and down the middle of the iron plaquettes. As a consequence, for the chalcogenides electronic hoppings of similar strength are to be expected along legs, rungs, and also plaquette diagonals.

Although the computational study of two-leg ladder one-orbital Hubbard and $t-J$ models were very successful in the context of the cuprates, the case of the

iron superconductors, even restricted to ladders, is more challenging. The reason is that multiorbital Hubbard models are needed and even powerful techniques such as the Density Matrix Renormalization Group (DMRG) [30] have difficulty in reaching sufficient accuracy for conclusive results. In spite of these limitations, a recent publication [31] reported progress in the study of a two-orbital model for $BaFe_2S_3$. In particular, the magnetic order with FM rungs and AFM legs was qualitatively understood and clearly reproduced over robust portions of parameter space [32]. However, the issue of pairing was more challenging due to severe size restrictions. In [31] it was assumed that high pressure causes doping of the two-leg ladders, a result supported by recent density functional theory calculations [33], and in agreement with the Cu-oxide two-leg ladders context where experiments showed [34] that indeed pressure transfers charge away from the ladders into chains effectively doping them. Under these assumptions an intriguing result was unveiled: using 2×8 clusters indications of binding of two holes were observed at intermediate values of the on-site Hubbard U repulsion, and for a realistic Hund coupling $J_H/U = 0.25$. Note that this binding does not occur at small U, so in principle it is outside the range of weak coupling expansions, and also does not occur in very strong coupling [31]. Remarkably, the reported binding happens in a finite and intriguing range of U/W, where W is the electronic bandwidth. However, the severe limitations in size prevented us from reaching final conclusions in [31] on whether the two-orbital model on a two-leg ladder does superconduct or not.

To improve on the situation described above there are two avenues that we are simultaneously pursuing. On one hand, the numerical aspects of the two-leg ladder model analysis described in the previous paragraph must be substantially improved. Progress has been made and pairing on 2×12 ladders has been confirmed recently (unpublished). Another avenue, pursued in the present publication, is to search for models or geometries with similarities to those of the real superconducting two-leg ladders but that would allow for the study of larger systems more comfortably.

In this context, in the present publication using DMRG we study a two-orbital model that is mathematically similar to that used before for $BaFe_2S_3$, but now defined simply on a *chain* as opposed to a two-leg ladder. When the binding energy is calculated vs. U/W the result, to be shown below, is similar to that found in the case of the two-leg ladder, with binding observed at intermediate couplings and with a shape of the binding energy curve vs. U/W resembling that previously reported. Due to this similarity, it is reasonable to believe that common physics causes the pairing tendencies both in ladders and in chains as long as two orbitals are active. The advantage of using chains, of course, is that much longer systems can be analyzed thus reducing size effects. For all these reasons, in this publication a systematic study of a two-orbital model defined on chains is presented, with emphasis on pairing and superconducting tendencies. The analysis is presented in a systematic manner, varying the many couplings and electronic densities and even further boosting pairing tendencies by introducing extra Heisenberg interactions. Overall, our analysis concludes that it is the Hund coupling J_H that primarily drives the pairing tendencies, supplemented by AFM tendencies between the effective $S = 1$ spins of the undoped sites. As explained below, it is known that there are unrealistic ranges of couplings where J_H explicitly boosts hole attraction. What is remarkable of our results described here is that *similar tendencies survive into the realistic regime* $J_H/U = 0.25$ *where the model is not explicitly attractive* because of the competition between J_H with the interorbital repulsion U'. These promising results are preliminary steps towards a clarification of the origin of pairing in iron-based superconductors, but more work is needed to establish definitely that pairing of electronic origin is active in two-orbital Hubbard models.

The organization of the manuscript is as follows. Section II provides details of the model, technique used, and observables measured. Section III contains the main results, addressing both magnetic and pairing properties of the model under scrutiny. Section IV contains our main discussion and conclusions.

II. MODEL AND METHOD

The multiorbital Hubbard model used in this publication is defined as

$$\begin{aligned} H = &-t\sum_{\substack{\langle ij\rangle \\ \gamma\sigma}}(c^\dagger_{i\gamma\sigma}c_{j\gamma\sigma} + h.c.) + U\sum_{i\gamma} n_{i\gamma\uparrow}n_{i\gamma\downarrow} \\ &+ (U' - \frac{J_H}{2})\sum_{\substack{i \\ \gamma<\gamma'}} n_{i\gamma}n_{i\gamma'} - 2J_H\sum_{\substack{i \\ \gamma<\gamma'}} \mathbf{S}_{i\gamma}\cdot\mathbf{S}_{i\gamma'} \\ &+ J_H\sum_{\substack{i \\ \gamma<\gamma'}}(P^\dagger_{i\gamma}P_{i\gamma'} + \text{h.c.}), \end{aligned} \tag{1}$$

where $c^\dagger_{i\gamma\sigma}$ ($c_{i\gamma\sigma}$) creates (annihilates) an electron at site i of a chain, with orbital γ (either a or b), and spin projection along the z-axis σ. The first term represents the kinetic energy of the electrons. Note that for simplicity, the 2×2 hopping matrix is the unit matrix i.e. only hoppings between the same orbitals is allowed. Although our overarching goal is the understanding of iron-based superconductors, these hoppings do not intend to represent the tunneling amplitudes of any particular material but they are chosen for simplicity. The second is the standard on-site Hubbard repulsion U between spins $\uparrow$ and $\downarrow$ electrons. The third term is the repulsion between electrons at different orbitals. As shown in many previous publications, besides the canonical U' repulsion the coupling strength affecting this term contains a contribution regulated by the Hund coupling J_H. Fourth is the

portion that explicitly shows the ferromagnetic character of the Hund interaction. The last term is the pair hopping. The number operator is defined as $n_{i\sigma\gamma} = c^\dagger_{i\sigma\gamma} c_{i\sigma\gamma}$ and the pair as $P_{i\gamma} = c_{i\gamma\uparrow} c_{i\gamma\downarrow}$. The standard relation $U' = U - 2J_H$ is assumed. While many of the results are for $J_H/U = 0.25$, considered realistic and used in the previous publication for ladders [31], in some of the results below the Hund coupling is varied. The bandwidth corresponding to the kinetic energy portion is $W = 4t$ and the Hubbard strength will be provided primarily as U/W. The hopping is the unit of energy $t = 1.0$, unless stated otherwise.

To obtain our results we use the DMRG technique with open boundary conditions with focus on the ground-state of the two-orbital chain, employing at least 1600 states. Most of the results are for a 32 sites two-orbital chain, unless stated otherwise, while some of the results were confirmed using up to 64 sites. Truncation error remain below $\sim 10^{-6}$ for all of our results [35].

We have measured several observables. The binding energy that is an indicator for pairing tendencies [36] is defined as

$$\Delta E = E_N + E_{N-2} - 2E_{N-1}, \tag{2}$$

where E_N, E_{N-1}, and E_{N-2} are the total ground state energy of the half-filled, 1-hole doped, and 2-hole doped systems. Here, $N = 2L$ with L the length of the chain. The real space charge and spin correlations are

$$N(R) = \frac{1}{N_R} \sum_{|i-j|=R} [\langle n_i n_j \rangle - \langle n_i \rangle \langle n_j \rangle], \tag{3}$$

$$Sp(R) = \frac{1}{N_R} \sum_{|i-j|=R} \langle \mathbf{S}_i \cdot \mathbf{S}_j \rangle, \tag{4}$$

where N_R is the number of neighbours at distance R from site i (namely, averages over pairs of sites at equal distance are performed). The Fourier transform of $Sp(R)$ is the spin structure factor $Sp(k)$

To study the effects of holes on the magnetic correlations, we define a projector operator $\mathcal{P}_{i\gamma}$ that projects out the portion of the ground state where site i and orbital γ are occupied [37]:

$$\mathcal{P}_{i\gamma} = c_{i\gamma\uparrow} c^\dagger_{i\gamma\uparrow} c_{i\gamma\downarrow} c^\dagger_{i\gamma\downarrow}. \tag{5}$$

To work in the Hilbert space corresponding to n_h number of holes at specific locations, we apply a product of projectors onto the ground state with n_h holes. For example, $\mathcal{P}_{6a}\mathcal{P}_{9b}|\psi_{N-2}\rangle$ projects out the occupied part of the two-hole ground state on orbital a at site 6, and on orbital b at site 9. We also calculate the local spin-spin correlations $\langle\psi|\mathbf{S}_{i\gamma} \cdot \mathbf{S}_{j\gamma'}\mathcal{P}|\psi\rangle/\langle\psi|\mathcal{P}|\psi\rangle$, where the maximum possible magnitude of the correlations is 3/4.

There are many possible superconducting pair correlations that one can explore for this system. Due to the local inter- and intra-orbital Coulomb repulsion, on-site pairing is not expected to dominate [36]. Thus, pairing operators for two electrons at nearest-neighbor (NN) sites i and $i+1$ will be considered in analogy with the approach taken in other purely electronic models where magnetic properties trigger pairing.

An intraorbital nearest neighbor pairing operators is

$$\Delta^{\gamma\gamma}_{nn,-}{}^\dagger(i) = c^\dagger_{i,\gamma,\uparrow} c^\dagger_{i+1,\gamma,\downarrow} - c^\dagger_{i,\gamma,\downarrow} c^\dagger_{i+1,\gamma,\uparrow}, \tag{6}$$

which creates a pair of electrons at nearest neighboring sites i and $i+1$ in orbital γ and forming a spin singlet. The corresponding pairing operator for the case in which the two electrons form a spin triplet is given by

$$\Delta^{\gamma\gamma}_{nn,+}{}^\dagger(i) = c^\dagger_{i,\gamma,\uparrow} c^\dagger_{i+1,\gamma,\downarrow} + c^\dagger_{i,\gamma,\downarrow} c^\dagger_{i+1,\gamma,\uparrow}. \tag{7}$$

Since the Hamiltonian is invariant under an orbital exchange only orbital symmetric combinations of the intraorbital pairing correlations have to be considered. An interorbital nearest neighbor pairing operator is given by

$$\Delta^{ab}_{nn,-}{}^\dagger(i) = c^\dagger_{i,a,\uparrow} c^\dagger_{i+1,b,\downarrow} - c^\dagger_{i,a,\downarrow} c^\dagger_{i+1,b,\uparrow}, \tag{8}$$

which creates two electrons at site i and orbital a and site $i+1$ and orbital b, forming a spin singlet (the orbital exchanged pairing operator is identical due to the orbital symmetry). The interorbital pairing operator that creates the electrons in a triplet state is given by

$$\Delta^{ab}_{nn,+}{}^\dagger(i) = c^\dagger_{i,a,\uparrow} c^\dagger_{i+1,b,\downarrow} + c^\dagger_{i,a,\downarrow} c^\dagger_{i+1,b,\uparrow}. \tag{9}$$

The pair-pair correlations are given by

$$\mathcal{O}^{\gamma\gamma'}_{nn,\pm}(R) = \frac{1}{2N_R} \sum_i \langle \Delta^{\gamma\gamma'}_{nn,\pm}{}^\dagger(i) \Delta^{\gamma\gamma'}_{nn,\pm}(i+R) \rangle, \tag{10}$$

where $\pm$ indicates if the pair is a spin triplet or singlet, and γ and γ' indicate orbitals a or b. Since the results explicitly presented in this manuscript are for the interorbital spin singlet $\mathcal{O}^{ab}_{nn,-}(R)$ and triplet correlations $\mathcal{O}^{ab}_{nn,+}(R)$, below we will use the notation $\mathcal{O}^{ab}_{nn,-}(R) \equiv S^{ab}_{nn}(R)$ and $\mathcal{O}^{ab}_{nn,+}(R) \equiv T^{ab}_{nn}(R)$, respectively. Analogous on-site pairing operators were also considered but their correlations always decayed faster than the dominant NN sites pair-pair correlation ($S^{ab}_{nn}(R)$ as shown below). For this reason, the actual expressions for on-site operators are not provided explicitly.

We have measured other observables as well. For example, by averaging the pair correlations over a finite intermediate portion of the chain we can reduce short distance effects, that sometimes lead to believe that pairing is dominant even if the long distance tail is small, and also to reduce boundary effects caused by the open boundary conditions. Here we define the pairing strength as

$$\bar{D} = \sum_{R=7}^{12} |S^{ab}_{nn}(R)|, \tag{11}$$

where we have used the spin-singlet nearest-neighbor combination explicitly because it will be shown below that it is dominant in our study.

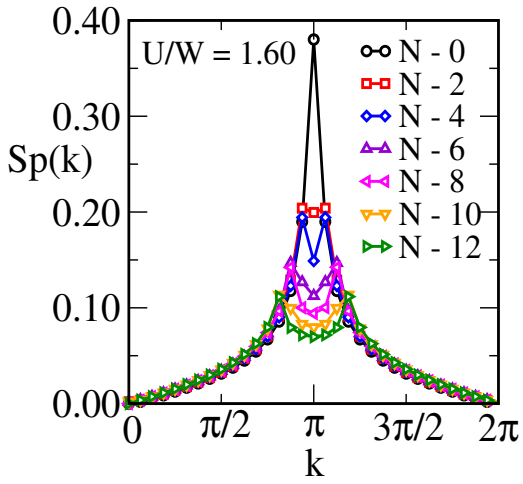

FIG. 1: (color online) Spin structure factor vs. wavevector k_x along the chain direction. Results correspond to $U/W = 1.60$, $J_H/U = 0.25$, various hole dopings as indicated, and employing a 32 sites chain ($N = 64$) and the DMRG technique. In this figure, and others not shown at several values of U/W, the peak at $k_x = \pi$ denoting staggered order at half-filling becomes incommensurate upon hole doping.

III. RESULTS

In this section, the main results will be described. The language to be used below should always be considered in the framework of one dimensional systems where long-range order is not possible. For example, expressions such as "staggered AFM order" indicate that staggered spin arrangements decay the slowest with distance as compared with other patterns, but eventually all correlation functions decay to zero with increasing distance in one dimension with short-range interactions.

As expressed before, we remind the readers that experimentally in the Fe-ladders superconductivity appeared with increasing pressure, not with explicit hole doping. However, similarly as in the case of the Cu-ladders, it is believed that pressure may lead to a rearrangement of charge particularly with regards to the average number of electrons at the iron atoms. This perception is supported by recent *ab-initio* calculations [33]. As a consequence, in our effort described below we will search for pairing indications by doping with holes the half-filled system, rather than modelling pressure directly.

A. Magnetic order and local moments

Let us start our computational analysis of the two-orbital Hubbard model defined in the previous Section by focusing on the magnetic order. Figure 1 contains the spin structure factor at $U/W = 1.60$, a coupling strength of much importance for pairing as shown below, for different number of holes. For the case of half-filling, $N = 64$ electrons for the 32-sites chain of focus in Fig. 1, the spin order is clearly of the staggered antiferromagnetic (AFM) form as expected. In this regime of Hubbard couplings the local spin at every site is already well developed and close to the spin-1 limit, as shown in panel (a) of Fig. 2 for most Hund couplings studied, with the exception of $J_H = 0$. Thus, this AFM correlations are compatible with the spin correlations of a Haldane spin-1 chain. Our study of a two-orbital Hubbard model, instead of a Heisenberg model, involves energy scales much higher than those typical of the integer-spin chains and for this reason we will not focus on subtle issues such as spin-gaps in the system. Panel (b) of Fig. 2 shows that together with the development of the spin-1 moments at every site also robust AFM correlations develop at least at short distances, again with the exception of $J_H = 0$.

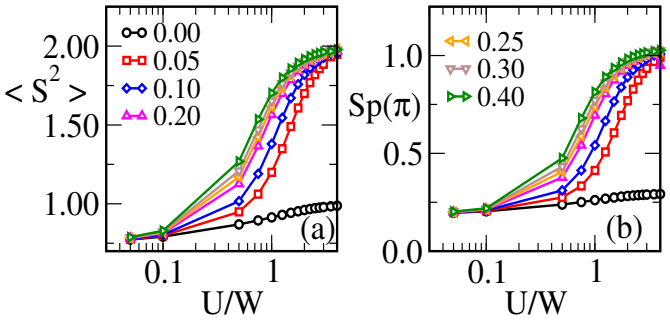

FIG. 2: (color online) (a) Spin squared $\langle S^2 \rangle$ and (b) staggered spin structure factor $Sp(\pi)$ vs. U/W for a half-filled 8-sites system using various Hund's coupling (J_H/U) as indicated. At zero J_H/U, local moments are not developed up to large U/W and therefore there is no robust magnetic ordering.

As the doping of holes increases, Fig. 1 illustrates that spin incommensurate (IC) correlations develop smoothly. While this spin IC order is compatible with spin excitations from the band dispersion in the kinetic energy portion of the model, note that $U/W = 1.60$ is already in intermediate coupling. Analysis of the spin-spin correlations "across holes" [38–40], to be shown in more detail below, indicate that the spins tend to arrange and couple in a manner qualitatively compatible with the exact results for the one-orbital Hubbard model at $U = \infty$ [41]. This arrangement is the most optimal to favor simultaneously the hole mobility and spin correlations, and it is qualitatively different from the analysis based on Fermi surface characteristics.

B. Hole pairs and their internal structure

The main result of this publication is that the model studied here presents a regime of hole pair binding that correlates with robust pair-pair correlations in a spin-singlet channel, as will be described below. Figure 3 shows the binding energy ΔE, as defined in Eq. 2, for the case of two holes added to half-filling, varying U/W at a fixed Hund coupling $J_H/U = 0.25$. Starting approximately at $U/W \sim 0.6$ and up to $U/W \sim 3.0$, the binding energy is negative indicative of the formation of

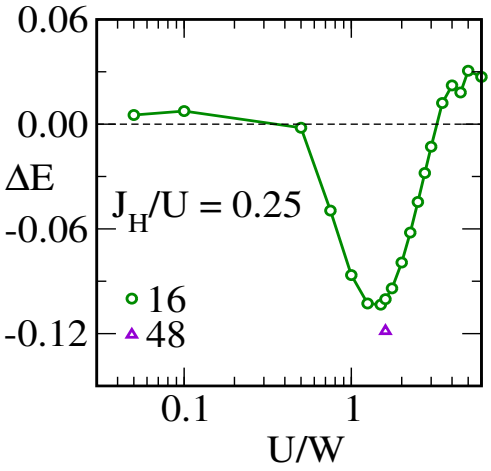

FIG. 3: (color online) Binding energy (ΔE) vs. U/W at a fixed $J_H/U = 0.25$, and using a 16-sites chain. For intermediate interaction strength, there is a wide range with negative binding energy indicating a region where holes pair.

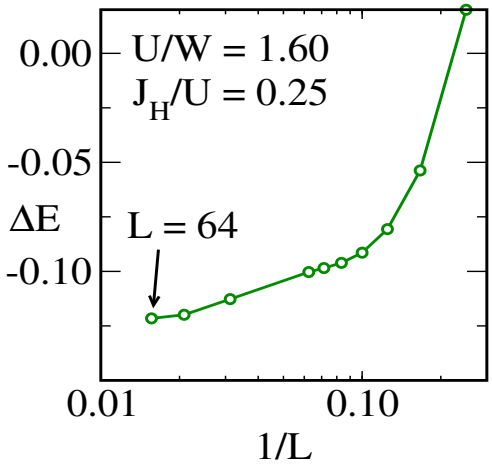

FIG. 4: (color online) Scaling of ΔE vs. inverse chain length ($1/L$) at coupling $U/W = 1.60$ where there is robust negative binding. In the bulk limit, ΔE remains negative according to the extrapolation of these results.

a bound state of two holes. Considering recent developments in the study of iron-based superconductors [6] this regime of U/W is realistic. Moreover, the Hund coupling value is also in a reasonable range for pnictides and chalcogenides that are well known for having a robust Hund-driven physics. The results in Fig. 3 were obtained using a 16-sites chain but they appear robust varying the length of the system. For instance, approximately at the minimum of the curve at $U/W = 1.60$ results for 48 sites are only slightly more negative than for 16 sites. Figure 4 contains a size scaling analysis of binding at $U/W = 1.60$ illustrating this conclusion. Our best efforts indicate that size effects are small and moreover with increasing chain length the binding magnitude slightly increases in absolute value. Thus, the bulk-limit binding energy at $U/W = 1.60$ appears to be close to -0.13 in hopping units.

Besides the surprising result that binding is possible even in the presence of a strong Hubbard U repulsion, it is interesting to remark the similarity of Fig. 3 with the binding results found before in the context of two-leg ladders (see Fig. 8 of [31]). In both cases, ladders (short sizes were studied in [31]) and chains, ΔE starts positive with increasing U/W, drops to negative at intermediate couplings where it remains into the strong coupling regime, and then it becomes positive again at abnormally large U/W. Note that the region where ΔE is positive is not important: in the bulk limit the energy of two holes that do not form a bound state should converge to the energy of two independent holes, rendering ΔE equal to zero. But the negative region of ΔE is physically realistic and representative of pair formation: two holes lower the energy of the system by being close to each other.

Figure 5 provides the electronic density using a 32-sites chain, corresponding to the orbital a (the results for b are identical, because the model is invariant if a and b are exchanged). For half-filling, the density is virtually

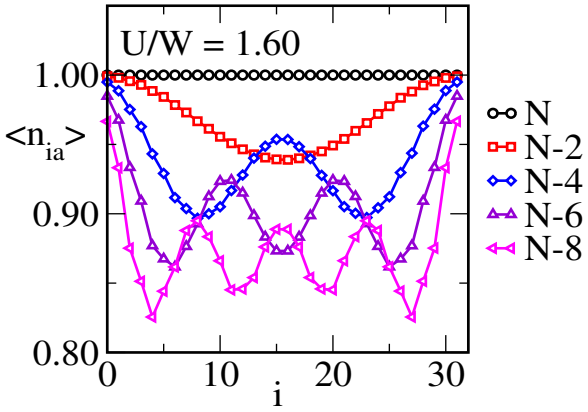

FIG. 5: (color online) Local charge density of orbital a at $U/W = 1.60$, i.e. in the binding region, using a 32-sites chain and $J_H/U = 0.25$. For a fixed number of holes n_h, we find $n_h/2$ number of "dips" in the charge density. Note that the charge density profile of orbital b is the same as that of orbital a, by symmetry.

equal to one at all sites. What is interesting is that for 2 holes, there is only 1 minimum indicative of the existence of a hole pair. For 4 holes there are 2 minima, for 6 holes 3 minima, and for 8 holes 4 minima. All these results are at least compatible with the existence of hole pair formation, as the binding energy indicates.

What is the internal structure of this pair? In Fig. 6 the probability of finding the second hole is shown when the first hole is projected to be at site 16, namely at the center of the 32-sites chain used, and at orbital a. It is clear that the probability for the second hole is the largest close to the first projected hole, compatible with pairing. Moreover, the second hole is primarily at orbital b if the first is at orbital a. Thus, the pairs unveiled here involve holes primarily located at different orbitals. This will be shown below to be compatible with the pair-pair correlation that is the most dominant in many portions of the

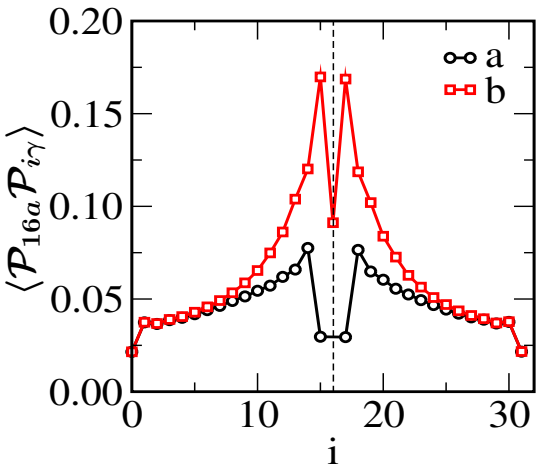

FIG. 6: (color online) Probability of finding a hole at site i and orbital γ given that the other hole is projected from the two-holes ground state to be at site 16, orbital a, of a two-orbital chain with 32 sites, at $U/W = 1.60$ and $J_H/U = 0.25$. The result is normalized to $\langle \mathcal{P}_{16a}\rangle$. We find the largest probability of the non-projected hole to be in the other orbital b and at the neighboring site. In the ladder analogy of the two-orbital chain (see Fig. 7), these dominant pairs are equivalent to pairs along the diagonal of effective plaquettes.

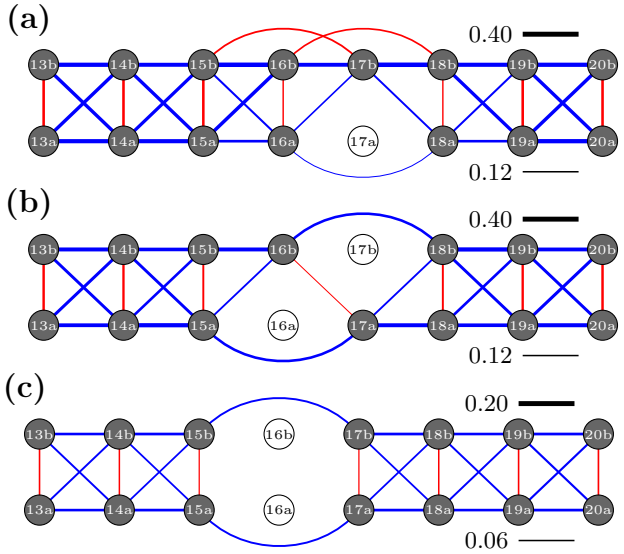

FIG. 7: (color online) Structure of the spin-spin correlations for fixed projected arrangements of holes, using hole configurations with large weight in the ground states. (a) is the one-hole case; (b) corresponds to holes along the effective plaquette diagonals (largest weight for two holes), while (c) are for holes along the effective rung. All results are obtained using 32 sites with two-orbitals at fixed $U/W = 1.60$ and $J_H/U = 0.25$. Blue lines correspond to AFM bonds while red lines are for FM bonds. Away from the holes, the expected pattern of FM effective rungs and AFM legs is recovered. In the fixed hole configurations of panels (b) and (c), the normalized probability of the holes configuration is $\langle \mathcal{P}_{16a}\mathcal{P}_{17b}\rangle/\langle \mathcal{P}_{16a}\rangle = 0.169$ and $\langle \mathcal{P}_{16a}\mathcal{P}_{16b}\rangle/\langle \mathcal{P}_{16a}\rangle = 0.0912$, respectively. In all cases there is a prominent "across the hole" AFM correlation. The case of two holes located along the same "leg" of the effective ladder has much smaller weight in the two-hole ground state and it is not shown.

phase diagram. Figure 6 also has prominent sharp peaks located at nearest-neighbors sites. Thus, the dominant hole configuration in the pair is that of holes separated by just one lattice spacing, located at different orbitals.

Projecting now one or two holes to particular locations and analyzing the spin-spin correlations in that framework leads to interesting conclusions. The results are shown in Fig. 7. First, note that once the two-orbital chain results are displayed representing each of the two orbitals by a chain, then this illustrates that two-orbital chains can be mapped formally into a special case of one-orbital two-leg ladders. This is interesting in several respects, but here we wish to emphasize the resemblance, once again, with the previously published results for two-orbital ladders [31]. Consider panel (a) for one hole: here the rungs of the effective ladder are ferromagnetic and the legs are AFM. Thus, once the results are plotted as in Fig. 7 the magnetic order resembles the "rung FM - leg AFM" of $BaFe_2S_3$ as reported in [31]. Also the AFM spin-spin correlation "across the hole" observed in early studies of models for cuprates [38–40] and also found more recently in models for iron-based ladders [31] is present in panel (a). From the spin perspective, "across the hole" AFM correlations are effectively equivalent to dropping sites of the chain, explaining the spin IC tendency in Fig.1 with increasing doping.

The results for two holes are equally interesting and also resemble those of previous investigations for real iron-based ladder models. Panel (b) contains the hole arrangement with the largest probability in the two-holes ground state. Similarly as in Fig. 10 of [31], the plaquette diagonal opposite to the projected holes is FM and the "across the hole" antiferromagnetism is robust. Panel (c) shows the case where the two holes are along the rung (i.e. on-site in the real chain). Panels (b) and (c) are smoothly connected: for instance by moving the electron at "17b" to "16b" in panel (c), panel (b) is recovered if the spin correlations follow as if they were "rubber bands" attached to the electrons. Previous studies in models for cuprates have unveiled similar physics.

Ending this subsection, we will discuss a subtle effect related with the spin quantum number of the two holes state. Employing Lanczos methods we studied the total spin of the two-holes state employing both periodic and open boundary conditions (PBC and OBC, respectively) using chains of length 4 and 6, at various Hund couplings and $U/W = 1.60$. The behavior is erratic: while for 6 sites and PBC the spin is always 0, for 4 sites with OBC it is always 1. The interpretation of these results is difficult because of the presence of the well-known edge states of Haldane chains when OBC are used. Considering the difficulty in distinguishing between intrinsic spin quantum numbers of a hole pair vs. those at the edge of a Haldane chain, we do not investigate further this topic and below

we study both singlet and triplet pair channels to find out which one dominates explicitly. The final result is that spin-singlet pairs are dominant suggesting that the spin 1 quantum number found for some two-holes chains originates in the edge states.

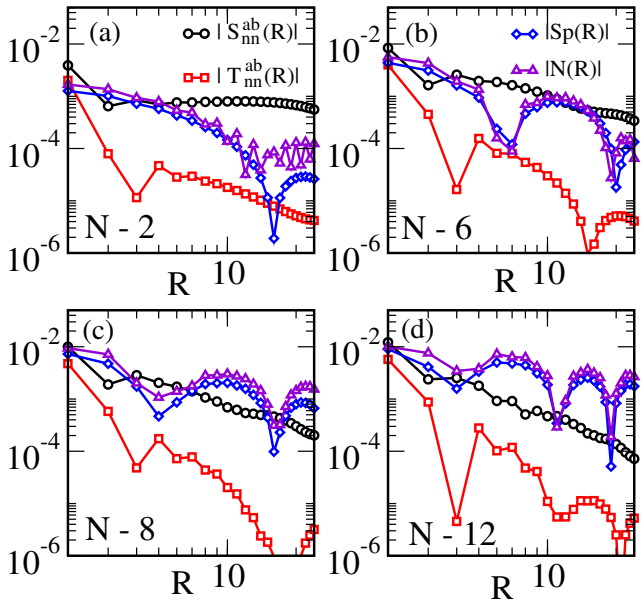

FIG. 8: (color online) Real-space decay of the pair-pair (singlet and triplet), spin-spin, and charge-charge correlations involving nearest-neighbor sites at fixed $U/W = 1.60$ and $J_H/U = 0.25$, and using a 48-sites chain. (a) corresponds to two holes doping, (b) to six holes doping, (c) to eight holes doping, and (d) to twelve holes doping.

C. Pair-pair correlations and tendency to superconductivity

The existence of hole binding at half-filling is often a precursor of superconducting tendencies increasing doping. For this reason we have measured the pair-pair correlations in all the channels described in Sec. II, and contrasted their behavior with increasing distance against density-density and spin-spin correlations to find which channel dominates. Representative results are shown in Fig. 8. Panel (a) contains results for 2 holes. Here the pair-pair correlations are robust in the spin-singlet channel when involving different orbitals and using nearest-neighbor sites, in agreement with the analysis of the internal structure of the pair in the previous subsection. The analogous spin-triplet pair correlations decay much faster, while spin and charge correlations are in between. However, in spite of the robustness of the singlet pair correlations in (a), the ground state only has two holes and these results, while promising, may be anomalous. More standard and exciting are the results in panel (b) with 6 holes and a nominal hole doping $x = 6/96 = 0.0625$ ($N = 96$ for a half-filled 48-sites cluster). The same spin-singlet inter-orbital NN-sites pair correlation dominates here as well, as in (a). The decay with distance is similar as in the charge and spin channels but only if the maxima is used for the latter. If, instead, the minima in charge and spin correlations are included in finding the most optimal fits then pair-pair correlations dominate. Note that the prominent oscillations in charge and spin correlations have been often reported before (for recent state-of-the-art efforts see [42]), although their origin is not fully clear; for the pair correlations a smoother behavior is often observed, as we found. As the number of holes increases, then the superconducting tendencies remain robust but diminish compared with spin and charge. In panel (c) with $x = 8/96$, the pair-pair decay with distance approximately follows the average of spin and charge indicating that they compete, while in panel (d) with $x = 12/96$, pairing is already less robust than charge and spin channels. In summary, in a range of doping near half-filling and for the clusters that we studied, the superconducting correlations appear to dominate, or at the minimum decay at a similar rate as spin and charge. With increasing hole doping the importance of the pair-pair correlations diminishes.

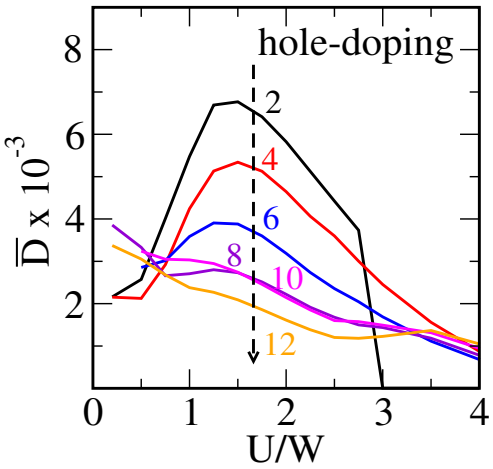

FIG. 9: (color online) Pairing strength $\bar{D}$ (see Eq. 11) vs. U/W, parametric with number of holes. A 32-sites chain is used and $J_H/U = 0.25$.

In Fig. 9 we show the pairing strength $\bar{D}$, defined in Eq. 11, as an indicator of the robustness of pairing correlations varying U/W for various number of holes. Clearly it is the intermediate range of U/W where pairing dominates the most – as found in the hole binding analysis – and also when the numbers of holes is small.

Note that the presence of robust superconducting correlations in Fig. 8 occurs in the region of pair binding shown in Fig. 3. Away from that region, for example at small Hubbard coupling such as $U/W = 0.2$ or at very large Hubbard coupling $U/W = 10$ pairing is not as robust as at intermediate couplings, as illustrated in Fig. 10. Thus, once again we arrive to the conclusion that the behavior of the binding energy and the pair correlation is compatible with one another.

For completeness, note that previous work also un-

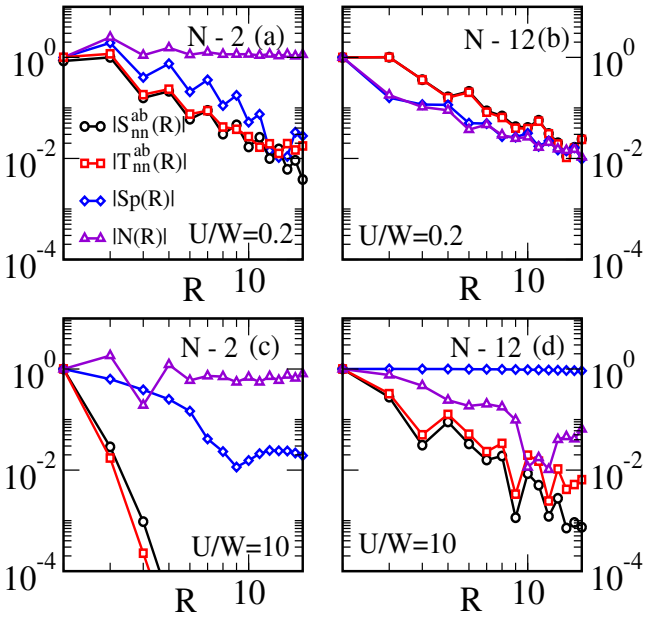

FIG. 10: (color online) Real-space decay of the pair-pair (singlet and triplet), spin-spin, and charge-charge correlations for two and twelve holes at $U/W = 0.2$ and 10.0, as indicated, and at $J_H/U = 0.25$ using a 32-sites chain. In all cases, the decay of the pairs is either faster or approximately equal to the spin and charge correlations. Thus, the pairing tendencies are robust at intermediate coupling, compatible with the conclusions regarding hole binding.

veiled tendencies towards pairing in electronic two orbitals models but under rather different circumstances. *(i)* For instance, in [43] Kondo models for $Y_{2-x}Ca_xBaNiO_5$ were studied using Lanczos and DMRG techniques, supplemented by AFM Heisenberg J terms. The emphasis was on ferromagnetism and phase separation but tendencies towards hole binding were also briefly reported. The signal for binding was strongest at high hole concentration such as $x = 0.4$ and robust values of J of order one. No pair-pair correlations were calculated, nor competition triplet vs. singlet was studied. *(ii)* In [44] two one-orbital Hubbard chains coupled by an explicitly ferromagnetic Heisenberg interaction were studied via bosonization and DMRG/Lanczos methods. Regions of singlet and triplet superconductivity were reported, but note that this model has an explicit Heisenberg effective attraction, without a U' repulsion (similar to our previous effort [45] to be discussed below). The goal in [44] was to study the singlet vs. triplet competition in superconductivity, unlike our efforts that focus on unveiling pairing tendencies from a complete two-orbital Hubbard model that is explicitly repulsive. *(iii)* In [46] a two-orbital Hubbard model at $U = \infty$ was studied with emphasis on the influence of the Hund coupling. When U' was included, charge-density waves were reported to dominate, while in the absence of U' but with robust J_H then singlet or triplet pairing dominates. Our analysis, on the other hand, focuses on a finite intermediate U/W range where surprisingly we found that singlet pairing dominates even in the presence of a realistic $U' > J_H$. As $U/W \to \infty$, we found that hole binding no longer occurs, as shown in Fig. 3, and the charge or spin channels dominate over pairing (see panels (c,d) of Fig. 10) compatible with [46]. *(iv)* In [47] results compatible with ours were produced via the exact diagonalization of a PBC 6-sites chain with emphasis on Luttinger liquid parameters using a two-orbital Hubbard model with a robust band splitting. *(v)* In [48] using the statistically consistent Gutzwiller approximation for a square lattice, conclusions similar to ours were reached, reporting a stable spin-triplet s-wave superconducting state for a two orbital degenerate Hubbard model. This occurs, like in our case, even in the case $U' > J_H$ and near half-filling.

D. Role of Hund coupling and magnetic moments

The origin of the pairing tendencies unveiled here is subtle and in this subsection we report some observations to help clarify this matter. More work is needed to fully comprehend this hole pair formation, so ours are just the first steps in that direction.

One important factor correlated with the pairing we are reporting is the presence of well-formed magnetic moments at every site. This is along the same direction as early studies of the $t - J$ model for cuprates [36] where holes form bound states to reduce the damage that mobile holes induce in an otherwise optimal antiferromagnetic arrangement. Each hole alters the spin order in a finite region, and pairing of holes reduces the size of the regions where spins are not properly arranged. This simple and well known notion must be at least part of the explanation for our results because pairing in ΔE, as shown in Fig. 3, occurs in regions where moments are well formed, as indicated in Fig. 2.

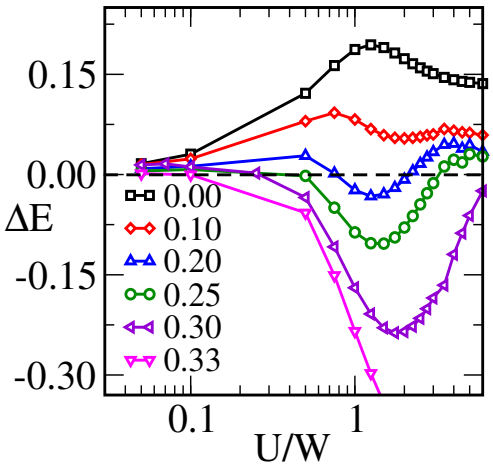

FIG. 11: (color online) ΔE vs. U/W parametric with J_H/U (inset) using an 8-sites chain with two orbitals.

In addition, we have observed that the Hund coupling in our model clearly is directly related to bind-

ing. Figure 11 shows the binding energy in a wide range of U/W parametric with J_H/U. At the smallest J_H/U shown, the binding energy is positive and pairs do not have a tendency to form. Consider now the special value $J_H/U = 1/3$. In this case $J_H = U'$ because of the relation $U = U' + 2J_H$. Thus, the natural repulsion U' for two electrons at different orbitals in the same lattice site is compensated by the natural tendency to bind induced by J_H. In fact for $J_H/U = 1/3$, and beyond i.e. $J_H/U > 1/3$, the binding energy ΔE is negative at all values of U/W.

The reader should note that the connection between the realistic regime $J_H/U < 1/3$ and the unphysical region $J_H/U > 1/3$ is non trivial. Naively, one may expect ΔE to be negative for all U/W for $J_H/U > 1/3$, and positive for all U/W for $J_H/U < 1/3$. However, the interpolation, while smooth, is more complex. Figure 11 shows that in the intermediate U/W range, the binding is negative for $J_H/U = 0.20$, 0.25, and 0.30, with a clear dip in the $U/W \sim 1-2$ range. This dip, being smoothly connected with the broad negative binding energy region of $J_H/U = 1/3$, must be caused by J_H attraction effects that somehow are not fully compensated by U' at intermediate couplings.

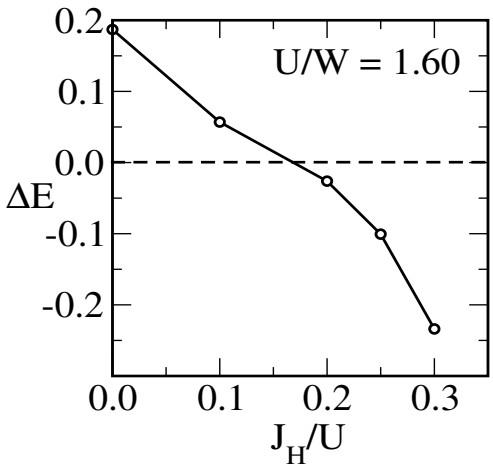

FIG. 12: (color online) ΔE vs. J_H/U at fixed $U/W = 1.60$ using 16 sites with two-orbitals. ΔE becomes significantly more negative as J_H/U is increased.

The "earlier" than anticipated attractive effects of J_H at intermediate U/W are explicitly illustrated in Fig. 12 where ΔE is shown at the optimal $U/W = 1.60$ of our focus, varying J_H/U. At least for the small system studied here, ΔE changes sign before $J_H/U = 0.2$ and it becomes increasingly negative with further increasing J_H. While the causal effect of J_H is clear, further work is needed to clarify how can this attraction overcome the U' repulsion in the intermediate coupling range. Moreover, the attraction channel favors spin-singlets involving different orbitals at nearest-neighbor sites. In fact, pairing in the spin-singlet inter-orbital NN-sites channels is enhanced as J_H increases as shown in panels (a,b) of Fig. 13. Thus, it is a subtle combination of the Hund interaction together with antiferromagnetic short-range order that induces singlet pairing in this one-dimensional multiorbital model. More work is needed to clarify this interesting effect.

E. Influence of additional inter-orbital Heisenberg interactions

For completeness, we have also added an extra term to the Hamiltonian in order to boost pairing tendencies. This term is simply a Heisenberg spin-spin interaction with strength J_D defined as

$$H_D = J_D \sum_{\langle ij \rangle} \mathbf{S}_{ia} \cdot \mathbf{S}_{jb}. \tag{12}$$

The motivation for adding this term is two folded. First, it plays a role similar to that of "J" in the standard $t-J$ model, and we know that increasing J increases pairing tendencies [36]. Second, the new term links the spins of two electrons located at NN sites and at different orbitals (note orbital indexes in Eq. 12), resembling the structure of the pairs that we have found above. In agreement with these expectations indeed we have observed that pairing tendencies in the dominant spin-singlet NN-sites inter-orbital channel are enhanced as shown in panels (c) and (d) of Fig. 13. A similar analysis adding instead a NN Heisenberg coupling between electrons in the *same* orbital only showed minor changes in the decay of the correlations (not shown). Clearly the electrons/holes in

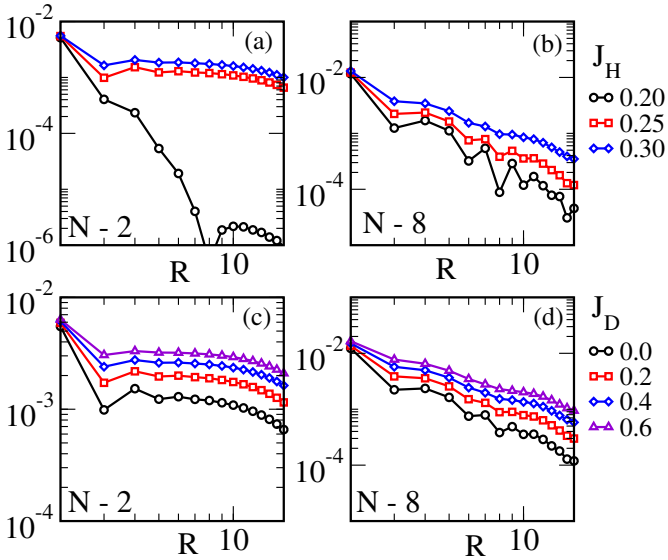

FIG. 13: (color online) Decay of pair-pair singlet correlations S^{ab}_{nn} at $U/W = 1.60$, for various Hund couplings in panels (a) and (b), and for various diagonal AFM Heisenberg couplings J_D in panels (c) and (d). Shown are results for 2 and 8 holes, as indicated, using in all cases a 32-sites chain and $J_H/U = 0.25$. Clearly increasing both J_H and J_D magnify the pairing tendencies.

the dominant pairs have a preference to be in different orbitals. Future studies of superconductivity in the two-orbital Hubbard model analyzed here can benefit from enhanced pairing effects by including J_D.

IV. CONCLUSIONS

In this publication we have investigated the magnetic, hole pairing, and superconducting properties of a two-orbital Hubbard model defined on a chain. The primary motivation is the recent report of hole binding tendencies in a similar model but defined on a two-leg ladder geometry [31], motivated by the discovery of superconductivity under high pressure in the ladder compound $BaFe_2S_3$ [11]. In that previous computational effort, the binding tendency was found to be negative, thus signaling pairing, but the results could not be confirmed beyond small systems 2×8. In addition pair-pair correlations were not measured in that early effort. In the present work much longer chains can be studied and a variety of correlation functions were measured and their decay with distance compared to decide which is dominant. In the same spirit as in [31], here our search for superconducting tendencies was based on hole doping while the experimental setup relied on pressure. The *ab-initio* calculations in [33] justify our theoretical approach because they reported that pressure leads to modifications in the average electronic density at the iron atoms.

Our results are interesting for several reasons. The data reported here for the binding energy resemble those of the ladder, but on chain sizes up to 64 sites. Size scaling shows that the results survive the bulk limit. Qualitatively both for ladders and chains it is the intermediate region of U/W were binding does occur. Having almost saturated magnetic moments is important together with a robust Hund coupling. Neither very weak nor very strong U/W coupling seem suitable for pairing, a conceptually interesting result. The absence of pairing at very large U/W may be related with competing ferromagnetic tendencies when holes are added, as in double exchange models. This line of research is being investigated at present.

Moreover, by measuring pair-pair correlations in the spin singlet channel, and using pair operators involving different orbitals and nearest-neighbor sites, a region of hole density and couplings was identified where superconducting correlations decay slower, or at least at the same rate, than spin and charge correlations. Having different orbitals and nearest-neighbor sites is compatible with the internal structure of the pair.

By varying the Hund coupling into the region believed to be unphysical where J_H becomes as large as U' (this occurs at $J_H/U = 1/3$ if the standard relation $U = U' + 2J_H$ is assumed [45, 49]), then an unexpected smooth continuity was observed between $J_H/U > 1/3$, where binding occurs at all values of U/W because J_H becomes an effective attraction when it overcomes U', and the region widely believed to be realistic $J_H/U \sim 0.25$. This smooth continuity occurs primarily at intermediate U/W couplings. Thus, for reasons that still need better clarification the effective J_H attraction at $J_H/U > 1/3$ can become operative even at smaller Hund couplings in a reduced U/W range. The chosen dominant channel involves holes in different orbitals, a spin-singlet combination, and nearest-neighbors sites.

The observation that pairing, charge, and spin correlations are sometimes of similar strength, as in panel (c) of Fig. 8 for $N - 8$ electrons (48 sites), suggests that future work should also address the possible formation of "pair density waves". These are subtle broken-symmetry states that intertwine charge density waves, spin density waves, and superconducting orders. In this state the superconducting order parameter is spatially modulated in such a way that the uniform component is zero or very small, but it has a strong oscillatory component [50–52].

In summary, these results contribute towards understanding pairing tendencies in quasi one-dimensional iron-based superconductors. Binding was found to occur at intermediate couplings, a regime that previous studies showed to be realistic for chalcogenides [6, 7]. There is plenty of work ahead. While superconducting correlations already appear to dominate at low hole doping, these results must be confirmed using even longer chains. Moreover, although it seems clear that a robust Hund coupling and robust magnetic moments are needed, developing an even more detailed qualitative understanding of the origin of pairing is important. Our group will continue working along these lines in the near future.

Acknowledgments

N.D.P., A.M., and E.D. were supported by the National Science Foundation Grant No. DMR-1404375. A.N. was supported by the U.S. Department of Energy (DOE), Office of Basic Energy Science (BES), Materials Science and Engineering Division. Part of this work was conducted at the Center for Nanophase Materials Sciences, sponsored by the Scientific User Facilities Division (SUFD), BES, DOE, under contract with UT-Battelle. G.A. acknowledge support by the Early Career Research program, SUFD, BES, DOE. Computer time was provided in part by resources supported by the University of Tennessee and Oak Ridge National Laboratory Joint Institute for Computational Sciences.

[1] D. C. Johnston, Adv. Phys. **59**, 803 (2010), and references therein.

[2] G. R. Stewart, Rev. Mod. Phys. **83**, 1589 (2011).

[3] P. J. Hirschfeld, M. M. Korshunov, and I. I. Mazin, Rep. Prog. Phys. **74**, 124508 (2011).
[4] D. J. Scalapino, Rev. Mod. Phys. **84**, 1383 (2012).
[5] A. V. Chubukov, Annu. Rev. Condens. Matter Phys. **3**, 57 (2012).
[6] P. C. Dai, J. P. Hu, and E. Dagotto, Nature Phys. **8**, 709 (2012), and references therein.
[7] E. Dagotto, Rev. Mod. Phys. **85**, 849 (2013), and references therein.
[8] F. Bondino, E. Magnano, M. Malvestuto, F. Parmigiani, M. A. McGuire, A. S. Sefat, B. C. Sales, R. Jin, D. Mandrus, E. W. Plummer, D. J. Singh, and N. Mannella, Phys. Rev. Lett. **101**, 267001 (2008).
[9] H. Gretarsson, A. Lupascu, J. Kim, D. Casa, T. Gog, W. Wu, S. R. Julian, Z. J. Xu, J. S. Wen, G. D. Gu *et al.*, Phys. Rev. B **84**, 100509 (R) (2011).
[10] D. Liu, W. Zhang, D. Mou, J. He, Y. Ou, Q. Wang, Z. Li, L. Wang, L. Zhao, S. He *et al.*, Nature Communications **3**, 931 (2012).
[11] H. Takahashi, A. Sugimoto, Y. Nambu, T. Yamauchi, Y. Hirata, T. Kawakami, M. Avdeev, K. Matsubayashi, F. Du, C. Kawashima, H. Soeda, S. Nakano, Y. Uwatoko, Y. Ueda, T. J. Sato, and K. Ohgushi, Nature Materials **14**, 1008 (2015).
[12] T. Yamauchi, Y. Hirata, Y. Ueda, and K. Ohgushi, Phys. Rev. Lett. **115**, 246402 (2015).
[13] Y. Hirata, S. Maki, J.-i. Yamaura, T. Yamauchi, and K. Ohgushi, Phys. Rev. B **92**, 205109 (2015).
[14] J. M. Caron, J. R. Neilson, D. C. Miller, A. Llobet, and T. M. McQueen, Phys. Rev. B **84**, 180409(R) (2011).
[15] H. Lei, H. Ryu, A. I. Frenkel, and C. Petrovic, Phys. Rev. B **84**, 214511 (2011).
[16] B. Saparov, S. Calder, B. Sipos, H. Cao, S. Chi, D. J. Singh, A. D. Christianson, M. D. Lumsden, and A. S. Sefat, Phys. Rev.B **84**, 245132 (2011).
[17] Y. Nambu, K. Ohgushi, S. Suzuki, F. Du, M. Avdeev, Y. Uwatoko, K. Munakata, H. Fukazawa, S. Chi, Y. Ueda, and T. J. Sato, Phys. Rev. B **85**, 064413 (2012).
[18] J. M. Caron, J. R. Neilson, D. C. Miller, K. Arpino, A. Llobet, and T. M. McQueen, Phys. Rev. B **85**, 180405(R) (2012).
[19] F. Du, K. Ohgushi, Y. Nambu, T. Kawakami, M. Avdeev, Y. Hirata, Y. Watanabe, T. J Sato, and Y. Ueda, Phys. Rev. B **85**, 214436 (2012).
[20] Q. Luo, A. Nicholson, J. Rincón, S. Liang, J. Riera, G. Alvarez, L. Wang, W. Ku, G. D. Samolyuk, A. Moreo, and E. Dagotto, Phys. Rev. B **87**, 024404 (2013).
[21] W. Lv, A. Moreo, and E. Dagotto, Phys. Rev. B **88**, 094508 (2013).
[22] C. Monney, A. Uldry, K. J. Zhou, A. Krzton-Maziopa, E. Pomjakushina, V. N. Strocov, B. Delley, and T. Schmitt, Phys. Rev. B **88**, 165103 (2013).
[23] Shuai Dong, J.-M. Liu, and Elbio Dagotto, Phys. Rev. Lett. **113**, 187204 (2014).
[24] Q. Luo and E. Dagotto, Phys. Rev. B **89**, 045115 (2014).
[25] Q. Luo, K. Foyevtsova, G. D. Samolyuk, F. Reboredo, and E. Dagotto, Phys. Rev. B **90**, 035128 (2014).
[26] E. Dagotto, J. A. Riera, and D. J. Scalapino, Phys. Rev. **45**, 5744 (1992).
[27] E. Dagotto and T. M. Rice, Science **271**, 5249 (1996).
[28] E. Dagotto, Rep. Prog. Phys. **62**, 1525 (1999).
[29] M. Uehara, T. Nagata, J. Akimitsu, H. Takahashi, N. Mori, and K. Kinoshita, J. Phys. Soc. Jpn **65**, 2764 (1996).
[30] S. R. White, Phys. Rev. Lett. **69**, 2863 (1992); U. Schollwöck, Rev. Mod. Phys. **77**, 259 (2005).
[31] N. D. Patel, A. Nocera, G. Alvarez, R. Arita, A. Moreo, and E. Dagotto, Phys. Rev. B **94**, 075119 (2016).
[32] Similar conclusions were reached via *ab−initio* calculations in R. Arita, H. Ikeda, S. Sakai, and M-T. Suzuki, Phys. Rev. B **92**, 054515 (2015). For spin-density functional calculation, see M-T. Suzuki, R. Arita, and H. Ikeda, Phys. Rev. B **92**, 085116 (2015).
[33] Yang Zhang, Lingfang Lin, Jun-Jie Zhang, Elbio Dagotto, and Shuai Dong, Phys. Rev. B **95**, 115154 (2017).
[34] Y. Piskunov, D. Jérome, P. Auban-Senzier, P. Wzietek, and A. Yakubovsky, Phys. Rev. B **72**, 064512 (2005), and references therein.
[35] See Supplemental Material at [URL will be inserted by publisher] to calculate the data needed to reproduce the results in this work.
[36] E. Dagotto, Rev. Mod. Phys. **66**, 763 (1994), and references therein.
[37] S. R. White and D. J. Scalapino, Phys. Rev. B. **55**, 6504 (1997).
[38] G. B. Martins, C. Gazza, J. C. Xavier, A. Feiguin, and E. Dagotto, Phys. Rev. Lett. **84**, 5844 (2000).
[39] G. B. Martins, C. Gazza, and E. Dagotto, Phys. Rev. B **62**, 13926 (2000).
[40] G. B. Martins, J. C. Xavier, C. Gazza, M. Vojta, and E. Dagotto, Phys. Rev. B **63**, 014414 (2000), and references therein.
[41] M. Ogata and H. Shiba, Phys. Rev. B **41**, 2326 (1990).
[42] Michele Dolfi, Bela Bauer, Sebastian Keller, and Matthias Troyer, Phys. Rev. B **92**, 195139 (2015), and references therein.
[43] J. Riera, K. Hallberg, and E. Dagotto, Phys. Rev. Lett. **79**, 713 (1997).
[44] T. Shirakawa, S. Nishimoto, and Y. Ohta, Phys. Rev. B **77**, 224510 (2008).
[45] J. C. Xavier, G. Alvarez, A. Moreo, and E. Dagotto, Phys. Rev. B **81**, 085106 (2010), and references therein.
[46] B. Ammon and M. Imada, J. Phys. Soc. Jpn. **70**, 547 (2001).
[47] K. Sano and Y. Ono, J. Phys. Soc. Jpn. **78**, 124706 (2009).
[48] M. Zegrodnik, J. Bünemann, and J. Spałek, New J. Phys. **16**, 033001 (2014),
[49] J.C. Xavier and E. Dagotto, Phys. Rev. Lett. **100**, 146403 (2008), and references therein.
[50] E. Berg, E. Fradkin, and S. A. Kivelson, Phys. Rev. Lett. **105**, 146403 (2010).
[51] J. Almeida, G. Roux, and D. Poilblanc, Phys. Rev. B **82**, 041102(R) (2010).
[52] E. Fradkin, S. A. Kivelson, and J. M. Tranquada, Rev. Mod. Phys. **87**, 457 (2015).